

# YALE PEABODY MUSEUM

P.O. BOX 208118 | NEW HAVEN CT 06520-8118 USA | PEABODY.YALE. EDU

## JOURNAL OF MARINE RESEARCH

The *Journal of Marine Research*, one of the oldest journals in American marine science, published important peer-reviewed original research on a broad array of topics in physical, biological, and chemical oceanography vital to the academic oceanographic community in the long and rich tradition of the Sears Foundation for Marine Research at Yale University.

An archive of all issues from 1937 to 2021 (Volume 1–79) are available through EliScholar, a digital platform for scholarly publishing provided by Yale University Library at <https://elischolar.library.yale.edu/>.

Requests for permission to clear rights for use of this content should be directed to the authors, their estates, or other representatives. The *Journal of Marine Research* has no contact information beyond the affiliations listed in the published articles. We ask that you provide attribution to the *Journal of Marine Research*.

Yale University provides access to these materials for educational and research purposes only. Copyright or other proprietary rights to content contained in this document may be held by individuals or entities other than, or in addition to, Yale University. You are solely responsible for determining the ownership of the copyright, and for obtaining permission for your intended use. Yale University makes no warranty that your distribution, reproduction, or other use of these materials will not infringe the rights of third parties.



This work is licensed under a Creative Commons Attribution-NonCommercial-ShareAlike 4.0 International License.  
<https://creativecommons.org/licenses/by-nc-sa/4.0/>



## **Estimating subsurface horizontal and vertical velocities from sea-surface temperature**

by J. H. LaCasce<sup>1</sup> and A. Mahadevan<sup>2</sup>

### ABSTRACT

We examine a dynamical method for estimating subsurface fields (density, pressure, horizontal and vertical velocities) in the upper ocean using sea-surface temperature (SST) and a climatological estimate of the stratification. The method derives from the “surface quasi-geostrophic” (SQG) approximation. The SST is used to generate a potential vorticity (PV) field which is then inverted for the pressure. We examine first the standard SQG model, in which the PV is assumed trapped in a delta-function layer at the surface. We then modify the model by introducing a subsurface PV which is proportional to the surface density and decays exponentially with depth. We derive the subsurface density from the hydrostatic relation, the horizontal velocities from geostrophy and the subsurface vertical velocities from the quasi-geostrophic omega equation.

We compare the predicted densities and velocities with those from a three-dimensional (3D) ocean model, and from *in situ* measurements in the Mediterranean, Eastern Pacific and the Azores Current. In most cases the standard SQG model predicts the qualitative structure of the subsurface flow. But it also underestimates its strength. The modified model yields better estimates of both the strength and vertical structure of the subsurface flow.

### 1. Introduction

Advances in satellite technology have greatly increased our ocean observing capability. Satellites provide estimates of sea-surface height (SSH) and temperature (SST), as well as chlorophyll content (SSChl, inferred from ocean color). These data are global in extent, and often available daily. It is highly desirable to use satellite data to estimate the surface and near-surface velocities, because these could be used to predict contaminant and biota transport.

The most common field used in this way is SSH which can be differenced to estimate geostrophic surface velocities. SSH measurements have generated a wealth of information about the surface fields (e.g. McPhaden, 1993; Chelton and Schlax, 1996; Stammer, 1997; Isachsen *et al.*, 2003). However, SSH has relatively coarse spatial and temporal scales; the average track spacing of the TOPEX instrument is a couple of degrees in longitude, and the

1. Norwegian Meteorological Institute, P. O. Box 43 Blindern, 0313 Oslo, Norway. *email: jlacasce@met.no*  
2. Department of Earth Sciences, Boston University, Boston, Massachusetts, 02215, U.S.A.

tracks repeat once every 10 days. Furthermore, it is not certain how the calculated velocities reflect those below the surface (i.e. exactly which vertical modes the height anomalies reflect).

SST and SSChl data have higher resolution, down to 1 km, and are provided as often as hourly. So these sets offer a potentially much more detailed view of the surface fields, in space and time. The problem is how to convert this information into velocities.

One approach is to use sequential fields to estimate the surface (horizontal) velocities. By tracking isoline displacements, one can estimate the velocities perpendicular to those lines. This is the idea behind the “maximum cross-correlation” (MCC) method (Emery *et al.*, 1986; Wahl and Simpson, 1990; Kelly and Strub, 1992; Breaker *et al.*, 1994; Zavialov *et al.*, 2002). The MCC method assumes that changes in surface temperature occur primarily from lateral advection, and estimates the surface velocities via a variational calculation. The method has been shown to produce reasonable estimates in various locations. However, it also has drawbacks; it is degraded by non-conservative processes (e.g. surface heating and cooling for SST, and local biological productivity for SSChl) and moreover is more successful predicting the flow perpendicular to the isolines than parallel. And the subsurface flow is not predicted, as with SSH differencing.

Hereafter we consider another way to use SST to predict velocities. This method requires only single realizations of the field (i.e. it does not involve temporal differencing) and also estimates the subsurface flow. The method derives from the “surface quasi-geostrophic” (SQG) model, which has been used previously to deduce the winds associated with temperature anomalies on the tropopause (Held *et al.*, 1995; Hakim *et al.*, 2002 and refs. therein). The idea stems from Eady’s (1949) model of baroclinic instability which involves the coupling between temperature anomalies at the surface and on the tropopause. The appeal of SQG as a dynamical system is that it has two, rather than three, dimensions facilitating computations.<sup>3</sup> The ocean surface is a region where these ideas are potentially applicable, because in most regions the ocean is deep and the velocities surface-intensified.

Besides being used for estimating velocities, the SQG model also has potential for use in assimilating SST into ocean models. Currently this is done by converting the SST into a 3-D temperature field using empirical functions (Tang *et al.*, 2004). The SQG model in contrast offers a *dynamical* means of generating that 3-D field. The empirical approach has been shown to be effective in some locations but less so in others, and it is believed that a dynamical approach is required (Tang *et al.*, 2004).

Hereafter we assess the SQG model by comparing with data obtained from a numerical simulation (with a non-hydrostatic ocean model) and from *in situ* measurements in three regions: the Mediterranean, the California Current and the Azores frontal region. We consider first the “standard” SQG model, in which the subsurface potential vorticity (PV) is

3. Some have, for instance, studied the properties of vortices under SQG (Held *et al.*, 1995). SQG vortices behave like those in 2-D turbulence, cascading energy to larger scales and temperature variance to smaller scales. But unlike in 2-D turbulence, front formation is common and filaments roll up, making new vortices.

assumed to be zero. Predictions using this model are often qualitatively correct, but produce fields which decay too rapidly with depth. We then explore using a modified SQG model, in which an empirical interior PV, derived from the surface temperature, is included. This addition greatly improves the strength of the subsurface flow.

Similar ideas were explored recently by Lapeyre and Klein (2006). They also applied the SQG model to predict subsurface fields in a primitive equation model simulation, and explored a modified version of the model. The present work compliments their study, and considers the application to actual ocean data.

## 2. The model

We wish to deduce the subsurface density from the surface density, to estimate the subsurface geostrophic velocities. Because we envision a use with satellite SST, we assume the density is solely a function of temperature; however the method is also applicable to surface salinity, should that become available in the future.

The model derives from the surface quasi-geostrophic (SQG) approximation, which involves several assumptions:

- The velocities are quasi-geostrophic (QG)
- The pressure is hydrostatic.
- The domain is small enough to ignore the latitudinal variation of the Coriolis parameter ( $f$ -plane approximation).
- The PV is confined to the surface and is constant (zero) in the interior.

Making the  $f$ -plane approximation implies restricting the application to domains roughly 100 km square. Larger areas would necessarily be subdivided into boxes and treated separately. The geostrophic and hydrostatic approximations require that the scales are not too small, less than roughly 1 km. The last assumption, that the interior PV is uniform, defines what we call the “standard SQG model.” We relax that assumption in Section 7. Under these approximations, all fields (velocities, temperature and pressure) can be derived from the surface temperature.

The QG approximation assumes the vertical velocity is small (of order Rossby number; Pedlosky, 1987) and that the density has a dominant component that varies only in the vertical:

$$\rho(x, y, z, t) = \rho_0 [1 - \alpha T_0(z) - \alpha T'(x, y, z, t)]$$

where  $T' \ll T_0$  (and  $\alpha$  is the thermal expansion coefficient). If this is so, the density (temperature) equation can be written as:

$$\frac{D_g}{Dt} T' + w \frac{d}{dz} T_0(z) = 0, \quad (1)$$

where  $D_g/Dt$  is the substantial derivative based on the geostrophic velocities,  $\mathbf{u}_g$ . So the temperature perturbation changes in response to advection by the geostrophic flow and to

up/downwelling across the background gradient. Note that we neglect vertical and horizontal mixing and sources/sinks of temperature, such as surface heating.

Taking the curl of the momentum equations and invoking continuity, we obtain the QG relative vorticity equation:

$$\frac{D_g}{Dt} \zeta_g = \frac{D_g}{Dt} \frac{1}{\rho_0 f} \nabla^2 p = f \frac{\partial}{\partial z} w \quad (2)$$

where  $p$  is the perturbation pressure. Combining Eqs. (1) and (2) yields an equation for the pressure:

$$\frac{D_g}{Dt} \frac{1}{\rho_0 f} \left[ \nabla^2 p + \frac{\partial}{\partial z} \left( F(z) \frac{\partial}{\partial z} p \right) \right] = 0, \quad (3)$$

where<sup>4</sup>

$$F(z) \equiv \frac{f^2}{g\alpha(dT_0/dz)}.$$

The quantity in the square brackets in (3) is the PV:

$$\frac{1}{\rho_0 f} \left[ \nabla^2 p + \frac{\partial}{\partial z} \left( F(z) \frac{\partial}{\partial z} p \right) \right] = Q. \quad (4)$$

If  $Q$  is known, one can invert Eq. (4) to obtain the pressure. This requires boundary conditions. At the surface ( $z = 0$ ), we match to the surface temperature by using the hydrostatic relation:

$$\frac{\partial}{\partial z} p(x, y, 0, t) = g\rho_0\alpha T'(x, y, 0, t). \quad (5)$$

We also demand that the solution vanish at depth ( $p \rightarrow 0$  as  $z \rightarrow -\infty$ ).

The standard SQG model assumes that  $Q = 0$  in the interior. This then is just the homogeneous solution of (4). That solution is easily obtained following a Fourier transform in  $x$  and  $y$ . If the mean stratification,  $T_0(z)$ , is linear, then  $F$  is constant and the pressure decays exponentially with depth:

$$p(x, y, z, t) = A(t) \frac{F^{1/2}}{\kappa} \exp\left(\frac{\kappa z}{F^{1/2}} + ikx + ily\right), \quad (6)$$

where  $\kappa = (k^2 + l^2)^{1/2}$  is the magnitude of the total wavenumber. Note that small scales (large wavenumbers) decay more rapidly than the large scales, implying the subsurface density resembles a *low-pass filtered version* of the surface field. Other stratifications are of

4. We retain dimensional equations to facilitate the application to data.

course possible.<sup>5</sup> More realistic profiles could also be used but require numerical computation (e.g. Kundu *et al.*, 1975; Flierl, 1978). Once we have the pressure, we can calculate the horizontal velocities, from geostrophy.

We will also calculate the vertical velocity. One way to do this is to use the temperature equation (1) (Hakim *et al.*, 2002). However this involves taking differences of the temperature field, requiring sequential realizations of the SST. An alternate approach is to use the quasi-geostrophic omega equation (e.g. Hoskins *et al.*, 1978; Pollard and Regier, 1992; Tintoré *et al.*, 1991; Pauley and Nieman, 1992; Viudez *et al.*, 1996; Rudnick, 1996; Shearman *et al.*, 1999), which requires only a single realization of the density. The omega equation can be written:

$$\nabla^2 w + F(z) \frac{\partial^2}{\partial z^2} w = 2 \nabla \cdot \mathbf{Q}, \quad (8)$$

where the “Q-vectors” are defined:

$$\mathbf{Q} \equiv -(dT_0/dz)^{-1} \left( \frac{\partial}{\partial x} \mathbf{u}_g \cdot \nabla T', \frac{\partial}{\partial y} \mathbf{u}_g \cdot \nabla T' \right).$$

The derivation of (8) is standard (e.g. Holton, 1992). The operator on the LHS of (8) is elliptic, implying  $w$  has the opposite sign as the divergence of  $\mathbf{Q}$ . To solve (8), we impose a rigid lid at the surface and at a prescribed lower depth. If  $F(z)$  is constant, one can Fourier transform in all three directions. Then (8) is easily inverted.

Hereafter we compare the standard SQG model with simulations from an ocean circulation model, and with *in situ* ocean observations. With the model, we have the full three dimensional velocity field for comparison, but with the field measurements we have only the density.<sup>6</sup> So in those cases we compare the predicted velocities with those generated from the *in situ* density.

### 3. Ocean circulation model

For the first test, we employ the ocean general circulation model described by Mahadevan *et al.* (1996). This is a three-dimensional, non-hydrostatic model, so that the vertical velocity is a prognostic variable. The model was run in a channel configuration,  $48 \times 96$  km in extent, with periodic east-west boundaries and solid north-south boundaries with zero heat flux. The model density, determined solely by temperature, was initialized with a front oriented east-west, and extending to approximately 250 m depth. The initial velocities were thus

5. If for example  $T_0(z)$  is exponential, the solutions can be obtained via the method of Frobenius:

$$G(z) = H \sum_{n=0}^{\infty} \frac{C}{n!(n+1)!} \frac{\kappa^{2n} e^{(n+1)z}}{F^n}, \quad C \equiv \left( \sum_{n=0}^{\infty} \frac{\kappa^{2n}}{F^n (n!)^2} \right)^{-1} \quad (7)$$

6. In some data sets, ADCP velocities are available. But we leave such comparisons to a later date.

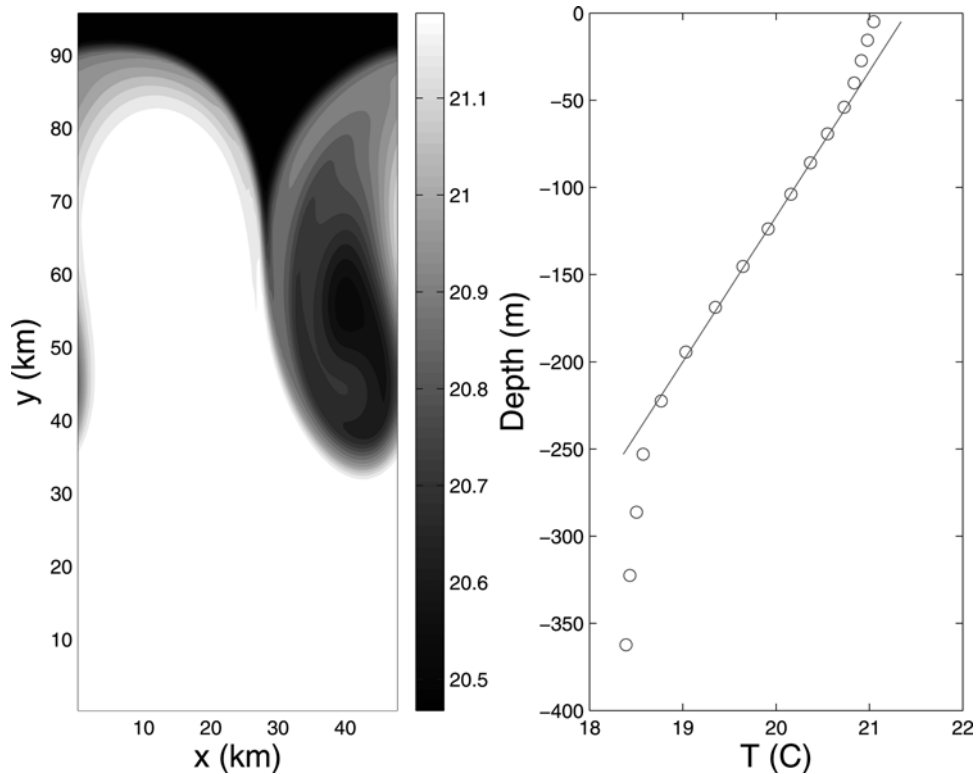


Figure 1. (a) Surface temperature contours from the non-hydrostatic model simulation during the pinching off of a cyclone from the unstable front. (b) The model areally-averaged temperature as a function of depth. The profile in the upper 250 m is approximated by a linear function.

purely zonal and geostrophic. After a short time the front became unstable, pinching off a cyclone on its southern side. A snapshot of the SST shortly after the eddy forms is shown in Figure 1. Note the sharp temperature front and also the asymmetry in the north-south direction, with a broader warm region in the south and a narrower cold region in the north.

The mean stratification, obtained by areally-averaging the temperature with depth is shown in Figure 1b. The profile exhibits a thermocline which is approximately linear to roughly 250 m depth. We thus take  $F$  to be a constant and impose the lower boundary, for the omega calculation, at 250 m.

Despite the front, the model velocities are very nearly geostrophic. The temperature contrast at the surface, roughly a half degree, is somewhat smaller than the 2.5 degree decrease over the upper 250 m. In addition the model PV (not shown) is surface-intensified; however it is not strictly surface-trapped (see also Section 7).

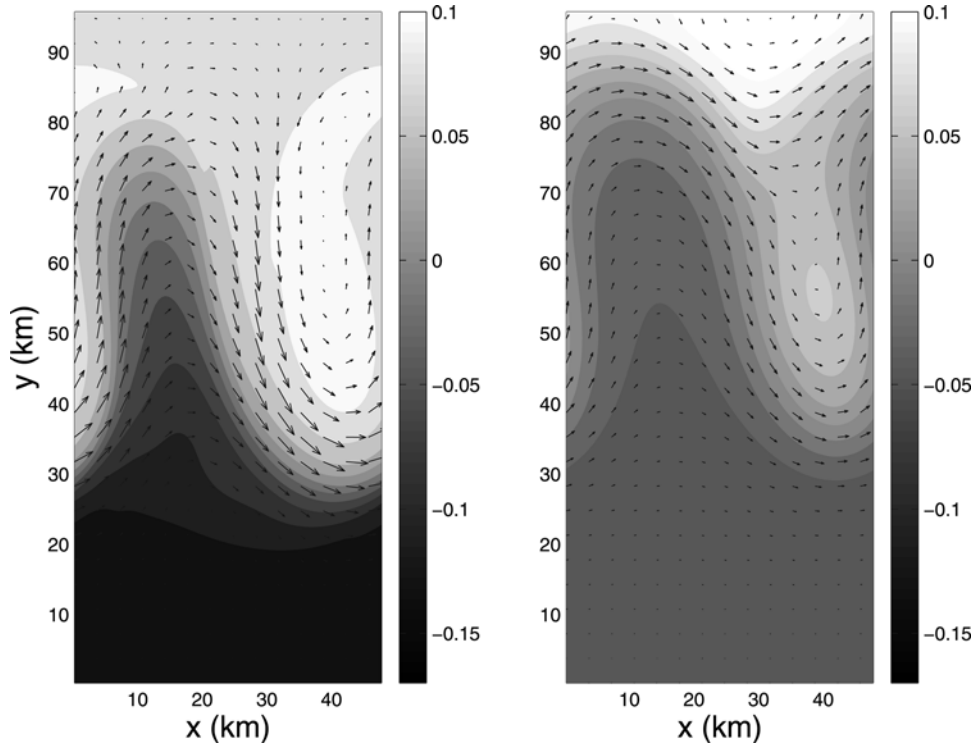


Figure 2. Model density anomaly (from the areally-averaged value) at 55 m depth (left panel) and that predicted by the SQG model (right panel). The horizontal velocity vectors are superimposed. The vectors correspond to a maximum velocity of 20 cm/sec. The maximum velocity in the SQG field is 12 cm/sec.

Figure 2 compares the density anomaly (the difference from the areal average) at 55 m depth with that predicted by the SQG model from the surface temperature.<sup>7</sup> The fields are qualitatively similar and moreover resemble low-pass filtered versions of the surface temperature. However, they also differ in several respects. The SQG density, like the model's surface temperature, is skewed, with a broader region of light water in the south. The model's density is more symmetric, with more dense water in the north. This suggests the model front slumps with depth (something that cannot be captured in the SQG idealization).

The horizontal velocity vectors are superimposed on the density contours. The flows are also qualitatively similar but differ in detail; the SQG model has eastward flow across the northern part of the dense tongue and weaker southward flow in the domain center. However the flow follows the front in both cases. The primary difference is that the SQG velocities are about half as strong as the model's (see also Fig. 19).

7. To derive density from temperature, we use the same thermal expansion coefficient as in the model.



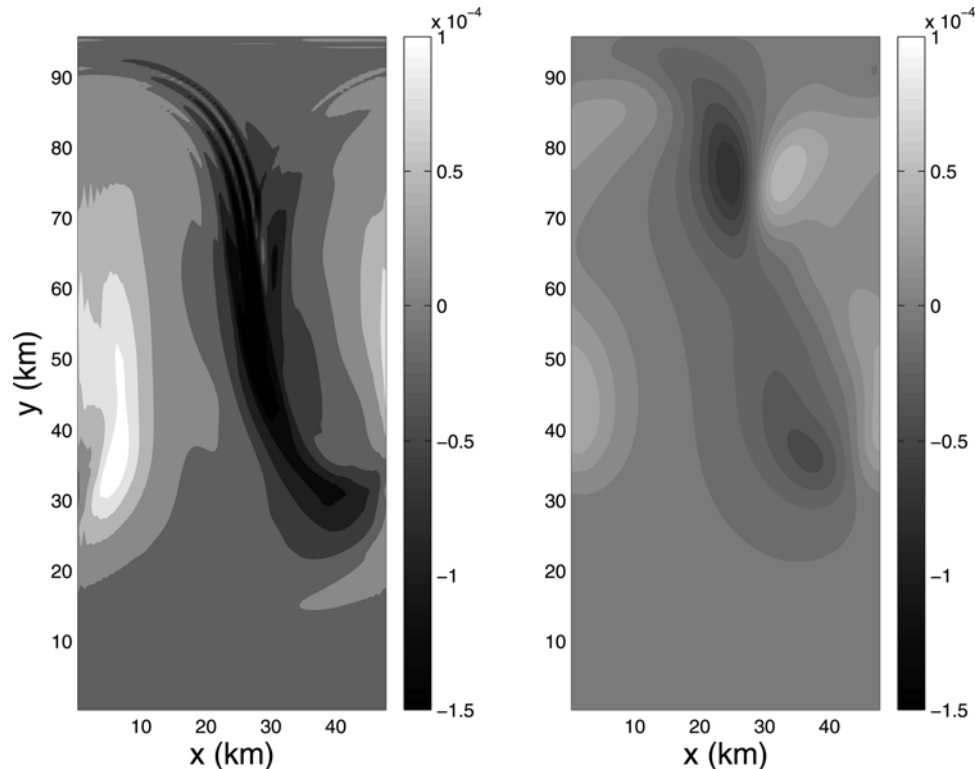


Figure 3. Vertical velocities (m/s) at 55 m depth in the model (left) and predicted by the SQG model (right).

Then there are the vertical velocities at 55 m (Fig. 3). Both the numerical and SQG fields exhibit downwelling in the center and upwelling at the edges, with the former aligned with the western edge of the cold tongue. But the structures in the SQG field are less sharp than in reality. In addition the SQG model exhibits structures (like the dipole in the northeast) not found in the model field. The predicted vertical velocities are also weaker than observed, by roughly one half.

Comparisons at other depths yield similar results. The primary difference is that the SQG densities, and hence the derived velocities, decay too rapidly with depth. So the velocities at 55 m are about half as strong as in the model, and they are proportionally weaker deeper down. As discussed in Section 7, this problem stems from the assumption of a surface-trapped PV.

Later on in the simulation the front collapses further, producing more eddies. The density and horizontal velocities at one such time are shown in Figure 4. Now there is also an anticyclone in the northwest, in addition to the cyclone in the east, and a zonal jet near  $y = 50$  km. The SQG fields capture the sense of the flow in most regions, but the predicted

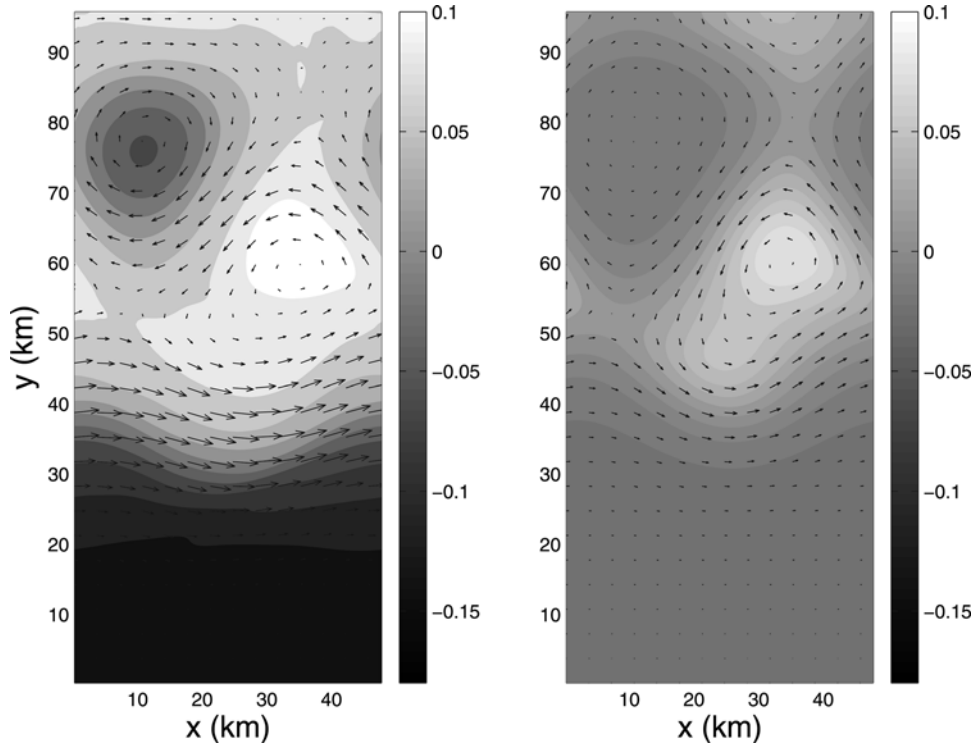


Figure 4. Model (left) and SQG-diagnosed (right) density anomaly at a later time at 55 m depth, with horizontal velocity vectors superimposed. The vectors are scaled using the maximum model velocity, which is 17 cm/sec; the maximum SQG velocity is 8 cm/sec.

density anomalies and velocities are again about half as strong as observed. The vertical velocities (Fig. 5) likewise show qualitative similarities. The SQG model correctly exhibits downwelling near  $y = 50$  km with upwelling nearby to the east. But the predicted fields are weaker by a factor of two and also exhibit some features not seen in the actual field (e.g. the dipole structure at  $y = 70$  km, which is evidently connected to a saddle point in Fig. 4).

#### 4. Alboran sea

Next we turn to three sets of *in situ* density data, derived from seasoar measurements. The seasoar is a tethered CTD which oscillates up and down in the near-surface waters, and measures temperature and salinity. We have only density measurements in these cases, so the primary goal will be to see whether SQG correctly captures the vertical structure of the density field. But we will also calculate the horizontal and vertical velocities from the *in situ* density, to compare with the SQG fields.

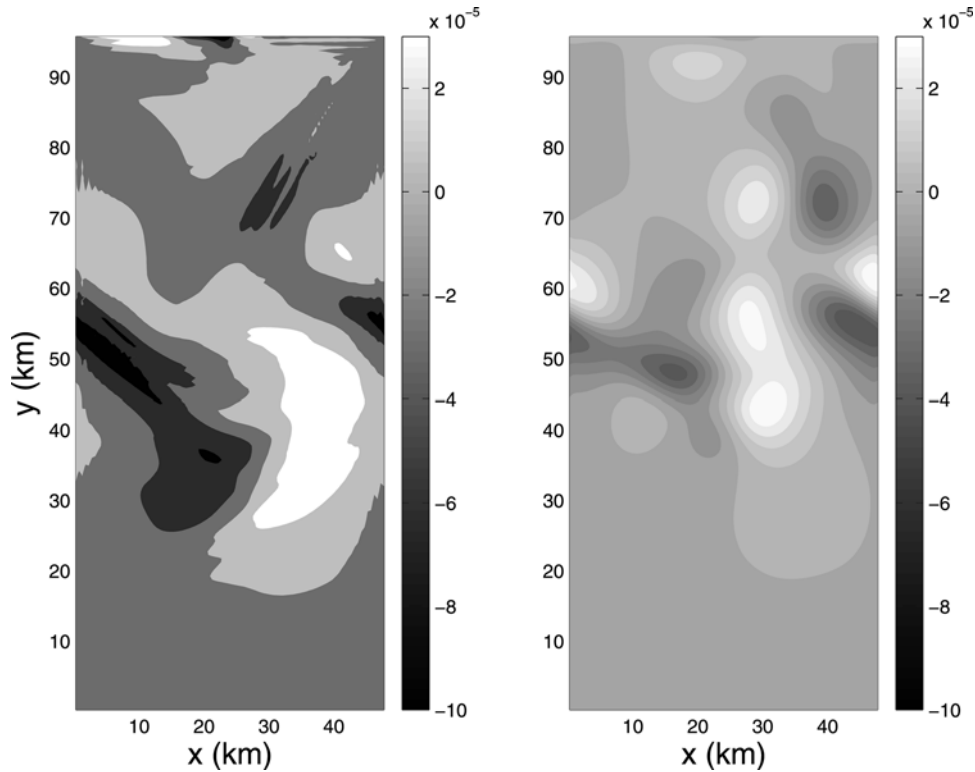


Figure 5. The 55 m vertical velocities (m/s) at the time corresponding to that of Figure 4.

For the SQG model, we use the surface temperature from satellite, where available. We also use the *in situ* density to estimate the mean stratification, by averaging over area. Note that the observed density also contains salinity contributions, which we neglect in the SQG model. In addition, the cruise data are obtained over several days, whereas satellite SST represents a snapshot of the surface on one day during the cruise.

The first data set, kindly provided by P. Velez-Belchi and J. Tintore, comes from a 1996 campaign in the Alboran Sea in the western Mediterranean (Velez-Belchi *et al.*, 2005). The satellite-derived SST at a time during the cruise is shown in Figure 6 (henceforth, SST refers to satellite-derived SST, unless mentioned otherwise). There is a large region of warm water adjacent to the African coast separated by a front from a cooler region near Spain. The subsurface density and temperature contours are very similar, suggesting the former is dominated by the latter, and both also resemble the satellite-derived surface temperature.

The area-averaged density is plotted against depth in Figure 7. The survey region itself encompasses a region only slightly larger than that occupied by the warm anomaly, but we assume the area-average is representative of the background nevertheless. We see that the

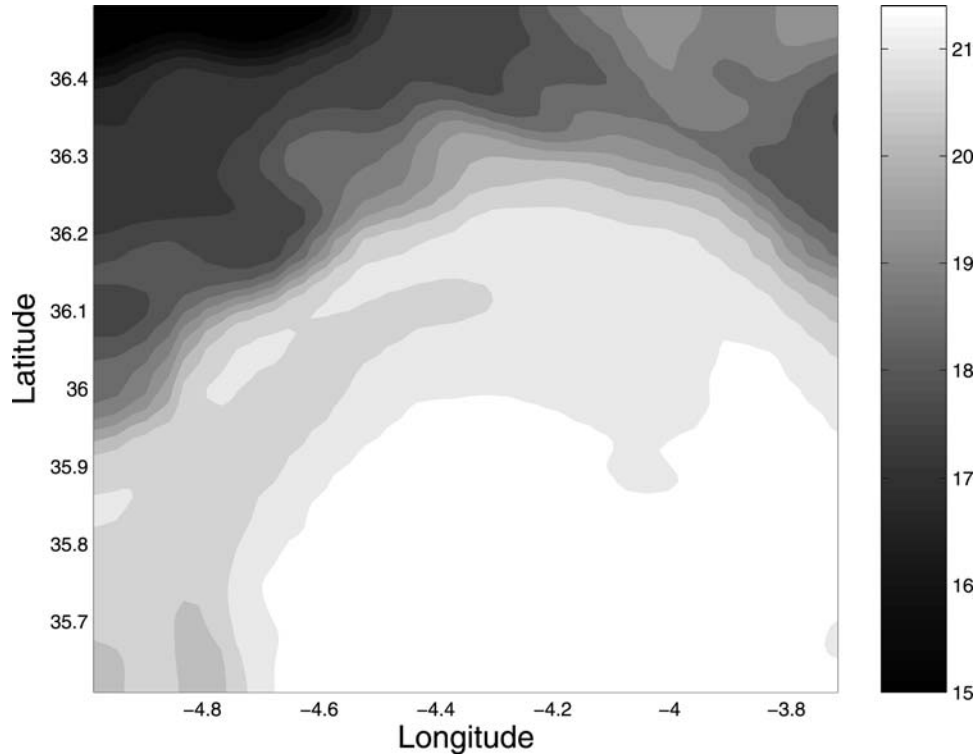


Figure 6. Surface temperature on October 3, 1996 in the Alboran Sea. The field has been smoothed recursively with a Laplacian filter.

stratification in the upper water column is well-approximated by a linear function, so we take  $F$  to be constant and restrict our attention to the upper 200 m.

In Figure 8 we compare the gridded seaosar densities with those predicted by the SQG model at three depths.<sup>8</sup> The SST field is from October 6, 1996, a date near the end of the seaosar survey. The structure of the SQG surface field is very similar to the observed (despite the slight difference in times). The deeper densities (middle and lower panels) are similar, with the bowl of light water receding southward. But while the *in situ* density anomaly actually strengthens somewhat with increasing depth, the SQG anomaly weakens.

Shown in Figure 9 are the velocities calculated from the *in situ* data and from the SQG model at 55 m depth. In addition to using the October 6 SST, we also use the October 3 field, from the beginning of the survey. The predicted flow is similar to the observed and mostly along the isopycnals. However, the SQG velocities are about 50–70 % of the observed,

8. We converted SST to density using a thermal expansion coefficient,  $\alpha = 4 \times 10^{-4} \text{ C}^{-1}$ , chosen so that the range of the surface density anomalies inferred from the SST matched the observed range at the surface.

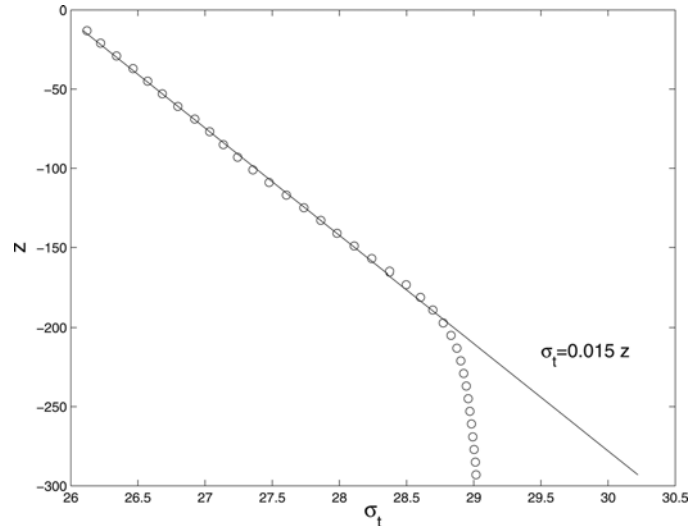


Figure 7. The areally-averaged density as a function of depth for the Alboran Sea data. The data derives from a smoothed, gridded set of seasoar data.

reflecting weaker density gradients in the SQG field. In this case too, stronger velocities are obtained with the modified SQG model (Fig. 18).

Figure 10 compares the vertical velocities derived from the densities. In both the observed and SQG-derived fields, the up- and downwelling occurs in compact regions along the front. The sizes and locations of the predicted maxima differ from the observed. However they also change substantially in the three days between October 3 and October 6, so some of the difference with the observed may be temporal variability. In addition, different smoothing was applied to the *in situ* and SQG-derived fields. The upwelling occurs primarily where the front is curved, and there are more such wiggles when less smoothing is applied.

## 5. California current

For the next comparison, we consider seasoar data collected off the coast of California, kindly provided by K. Shearman. Shearman *et al.* (1999) describe the corresponding fields, and also diagnose the vertical velocities using the omega equation formulation.

The satellite-derived SST for the region at the time of the cruise is shown in Figure 11. There are cold filaments emanating from the California coast and extending into the survey region. These features greatly affect the local density, as discussed by Shearman *et al.* (1999).

The mean stratification, inferred from the seasoar data, is shown in Figure 12. Above 30 m, the stratification is nearly homogeneous. Below that it is exponential, with an e-folding scale of about 80 m. We could take the background stratification to be exponential, as noted in

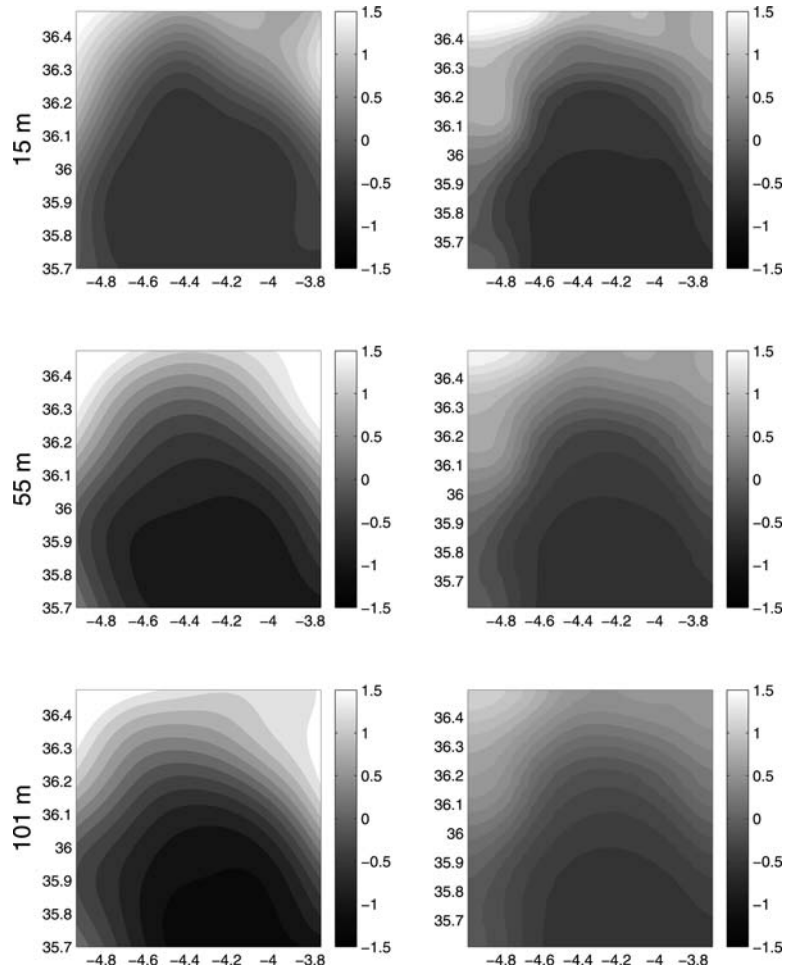


Figure 8. The density anomalies in the Alboran Sea, from the gridded sea surface temperature data (left) and from the SQG projection of the SST (right, from the October 6, 1996 field). The depths shown are 13 m (top), 55 m (middle) and 101 m (bottom). The density and SST data sets have been smoothed independently.

Section 2, but for simplicity we assume it to be linear. We also take the lower boundary for the omega calculation to be at 150 m.

The SQG-derived densities and horizontal velocities at 20 and 60 m are shown in Figure 13. The observed field at 20 m has a cold tongue extending from the north across the middle of the domain. The same feature is seen in the SQG-derived density. But while the horizontal velocities largely follow the isopycnals in the predicted field, they do not in the data; rather there is eastward flow in the central and southern domain, across the isopycnals.

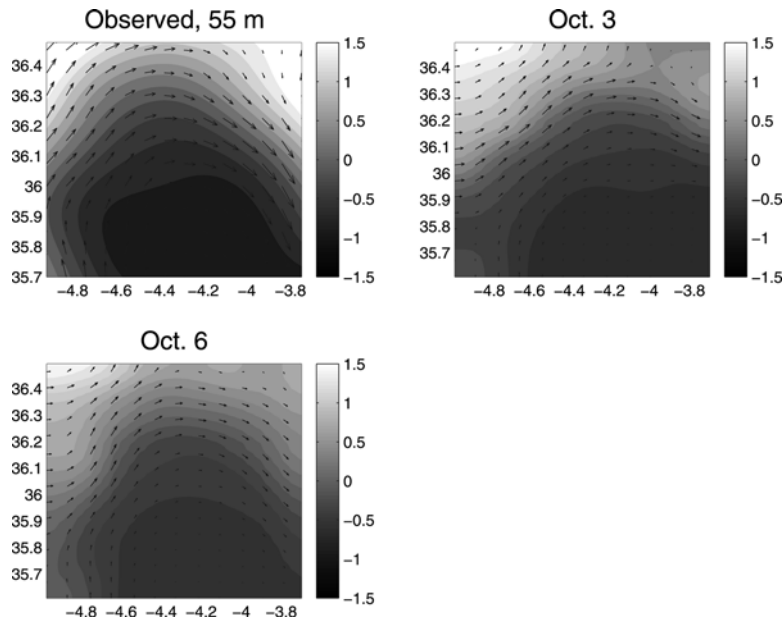


Figure 9. The horizontal velocity fields at 55 m depth derived from the gridded *in situ* data (upper left) and from two SST fields. The velocity vectors are scaled using the maximum observed velocity of 1.14 m/sec; the maximum SQG velocities are 70 and 52 cm/sec, respectively.

In addition, the SQG velocities are much weaker than observed, by an order of magnitude at 60 m.

The reason for the differences is seen in the lower left panel: there is a *second* cold tongue entering from the upper right. There is evidence for this deeper tongue in the 20 m density, but it is much stronger at depth. The observed flow at 60 m is mostly along the isopycnals defining this structure, and it is this which causes the cross-isopycnal flow at 20 m. The SQG-derived flow at 60 m instead looks like that at 20 m, only weaker, and so is very different from observed. The vertical velocities (not shown) are similarly affected by the subsurface cold tongue.

The SQG model fails here because of its assumption of conservative temperature dynamics at the surface. Surface forcing has created a mixed layer and thereby obscured the deeper tongue, and without a strong surface signature, the SQG model cannot reproduce the subsurface flow. SQG does succeed in approximating the flow in the mixed layer, but it fails to capture the vertical structure.

## 6. Azores front

The last comparison involves seaosar data kindly provided by D. Rudnick and described in Rudnick and Luyten (1996) and Rudnick (1996). This comes from one of three surveys

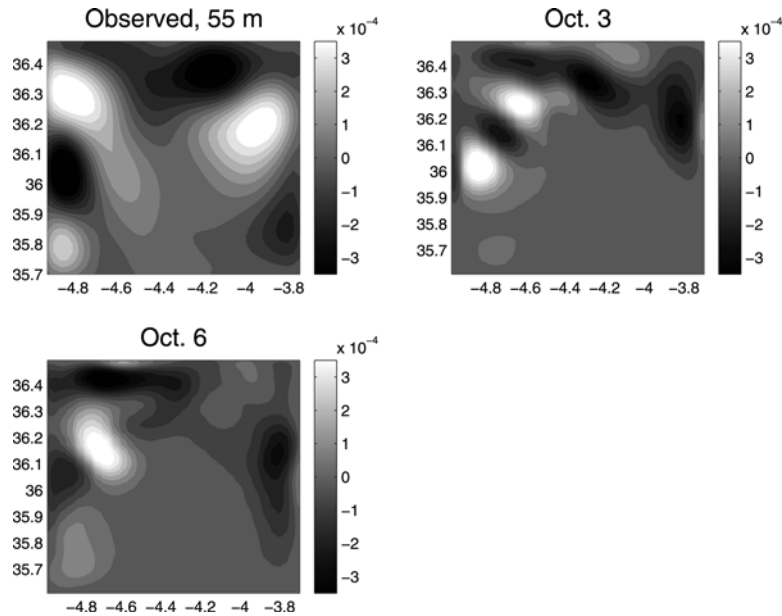


Figure 10. The vertical velocities (m/s) at 55 m depth from the *in situ* data (upper left) and from two SST fields. The *in situ* and SQG densities have been smoothed independently, and this affects the size of the upwelling centers. The *in situ* vertical velocities are estimated using the same routine with the SQG-derived density (and are very similar to those derived by Viudez *et al.*, 1996).

of the Azores Front in 1991–2, to measure subduction in the region. The mean stratification, derived from the area-averaged density, oscillates with depth but can be roughly approximated by a linear function (Fig. 14). Unlike with the California Current profile, there is no homogeneous layer at the surface.

We were unable to obtain a suitable satellite SST field for this region and time, so we used instead the temperature measured by the seasoar itself (at 4 m depth). This suffices for testing the vertical structure of the density field. As with the Alboran Sea data set, we chose the thermal expansion coefficient so that the density contrasts (inferred from the temperature alone) agree with the observed surface values; specifically we took  $\alpha = 1.5 \times 10^{-4} \text{ C}^{-1}$ .

The observed density and horizontal velocities at 68 m depth (Fig. 15) reveal denser water to the north and lighter water to the south, with bands of intensified flow tilted slightly from the east-west direction. The SQG fields are similar, with the density increasing to the north and the flow intensified in two tilted bands. But the predicted fields are once again weaker. The maximum SQG velocity is 32 cm/sec, compared to 52 cm/sec in the observed field.

The vertical velocities inferred from the densities are shown in Figure 16. In both cases there is localized up- and downwelling near the front in the domain center. These maxima are associated with curved isopycnals, as in the previous examples. But the predicted velocities are weaker than observed, like the horizontal velocities.



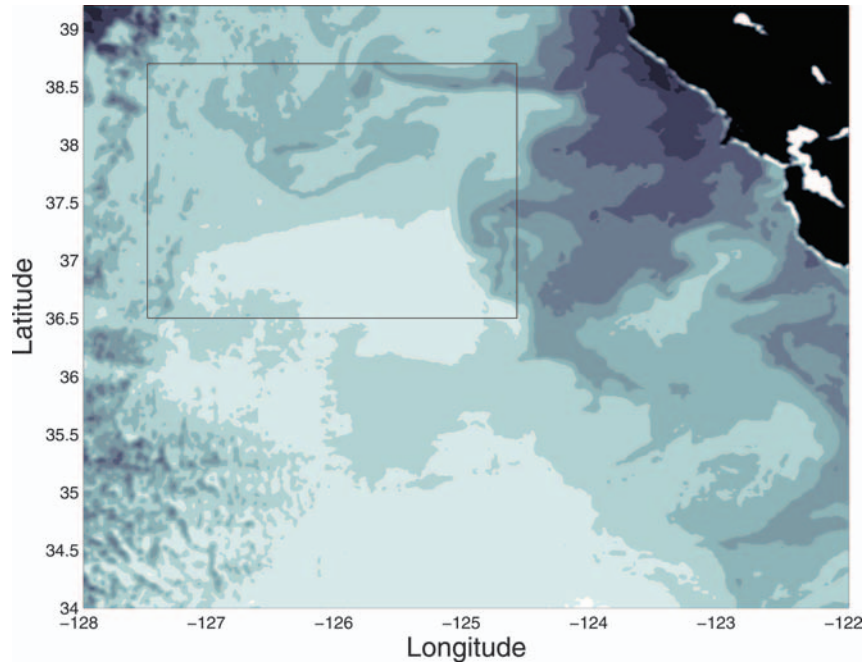


Figure 11. Surface temperature on June 29, 1993 off the coast of California. The region surveyed and described by Shearman *et al.* (1999) is indicated by the box. The satellite SST has been smoothed with a Laplacian filter.

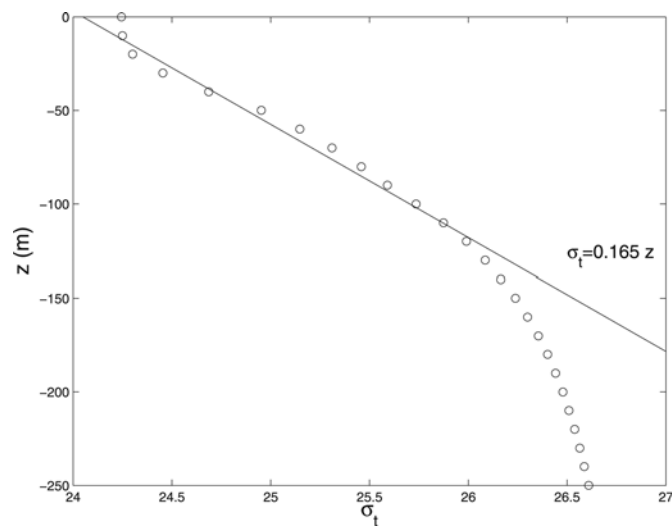


Figure 12. The areally-averaged density as a function of depth for the gridded California Current data. A linear function is used to approximate the stratification, despite the homogeneous layer near the surface and the fact that the profile is nearly exponential below 30 m.

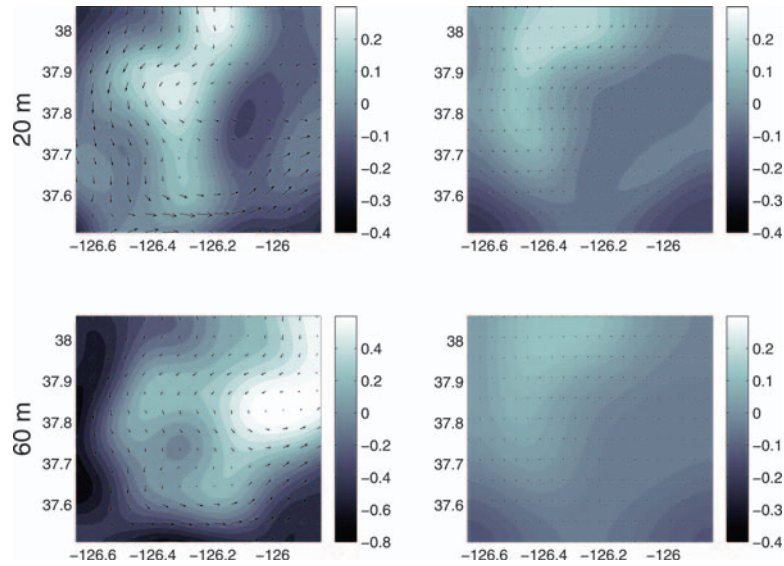


Figure 13. The densities and horizontal velocities at 20 and 60 m depth from the gridded seasonar data (left) and predicted from SST (right). The velocity vectors are scaled using the maximum observed 20 m velocity of 82 cm/sec; the maximum 60 m observed velocity is 66 cm/sec, while the SQG velocities, 11 and 5 cm/sec, are much smaller. Note the color scale in the lower left panel is different than the others, because of the cold tongue entering from the right.

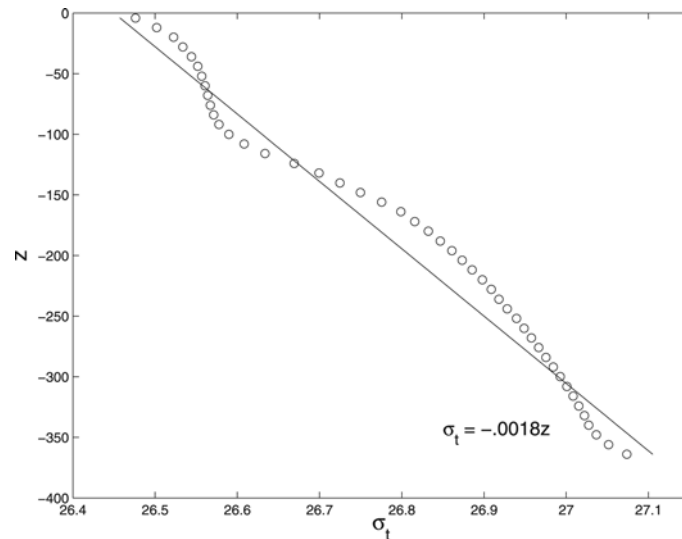


Figure 14. The areally-averaged density as a function of depth for the Azores current data, gridded by D. Rudnick. The linear approximation for the stratification is indicated.

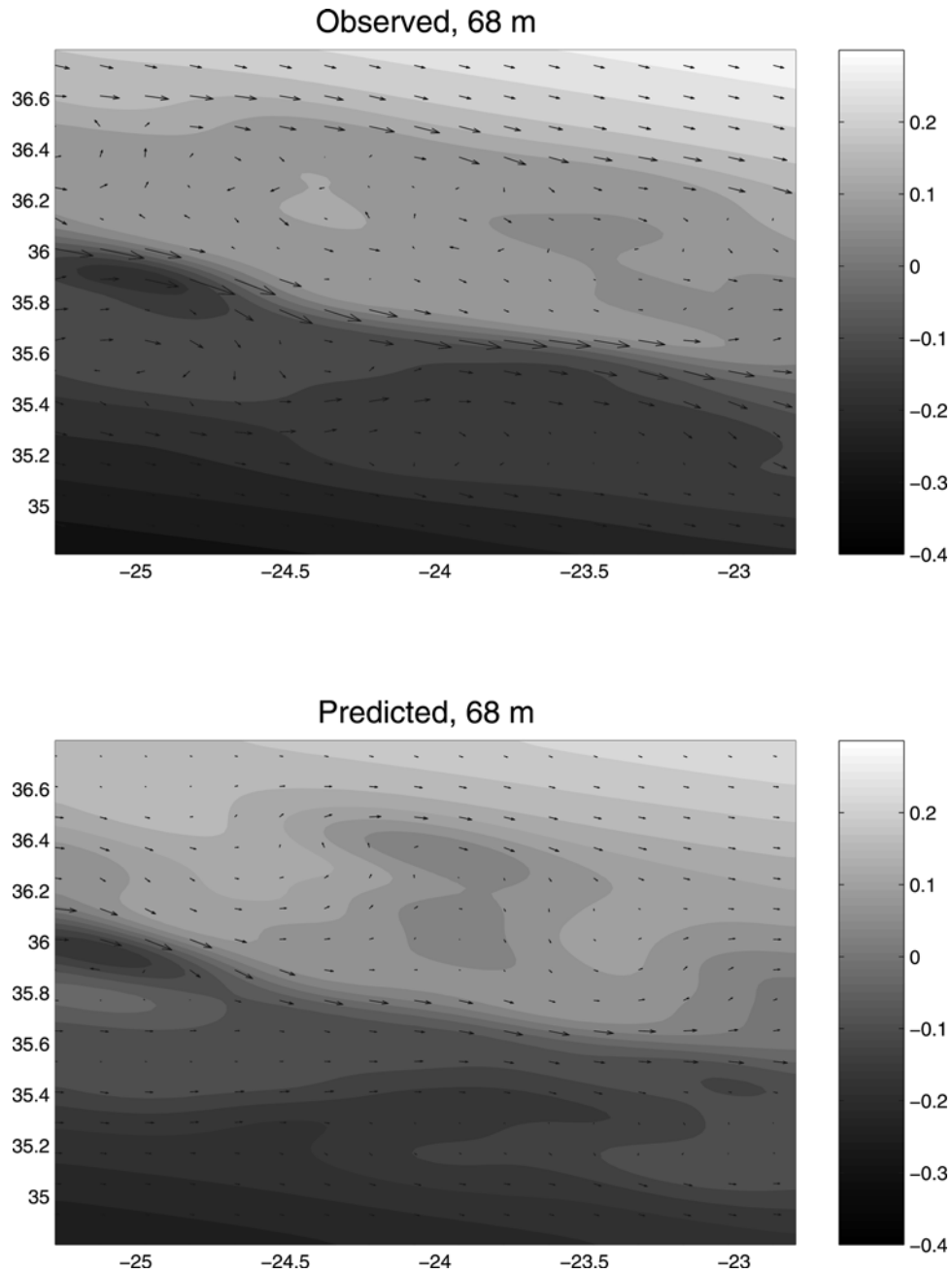


Figure 15. The densities and horizontal velocities at 68 m depth from the gridded Azores seaoar data (upper panel) and those predicted from the shallowest (4 m) temperature field. The velocity vectors are scaled using the maximum *in situ* velocity of 52 cm/sec; the maximum SQG velocity is 32 cm/sec.

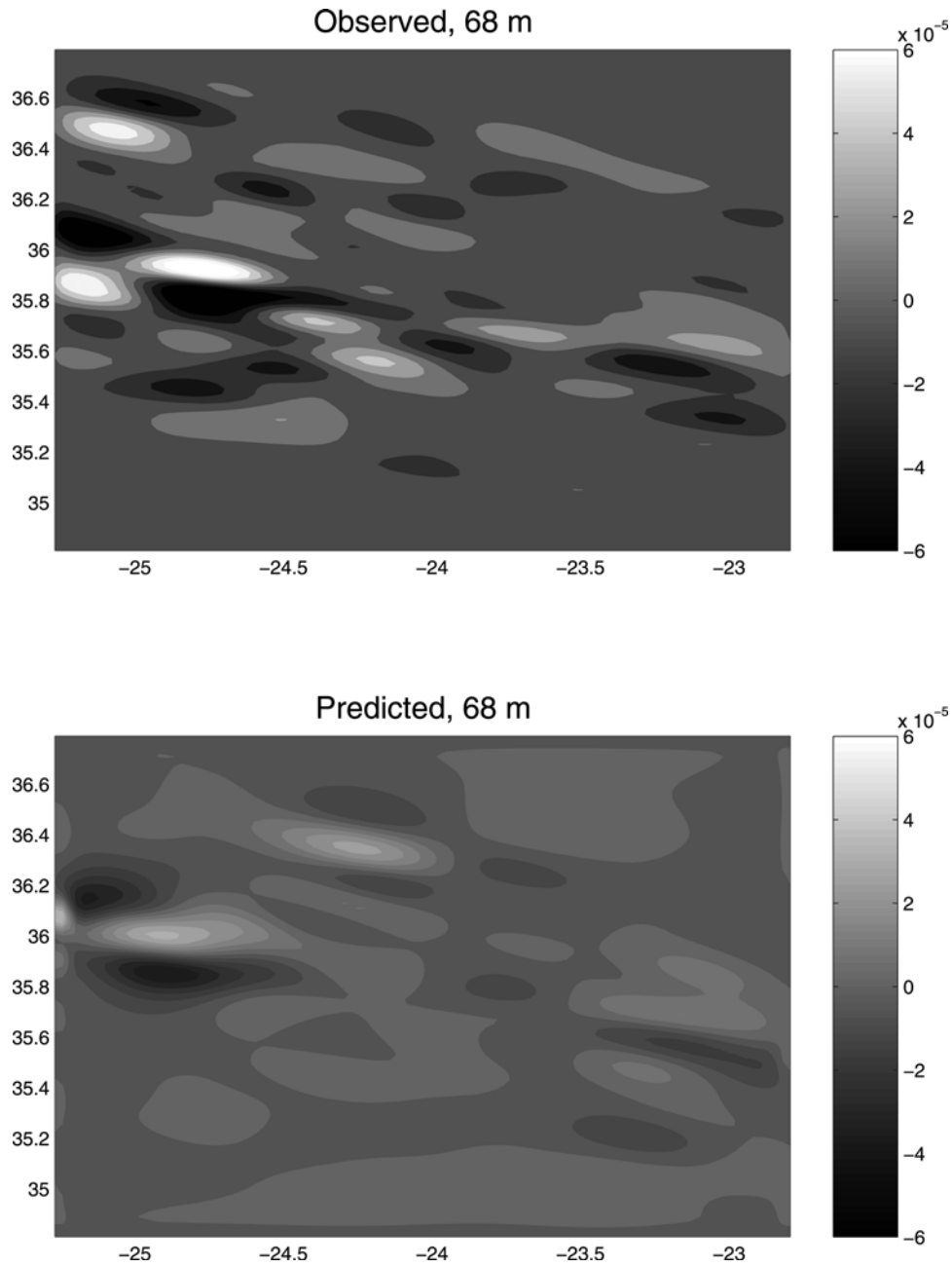


Figure 16. The vertical velocities at 68 m depth inferred from the *in situ* and SQG-derived density fields from the Azores season data. The *in situ* estimate is very similar to that calculated by Rudnick (1996), despite his using different boundary conditions for the  $\omega$ -equation.

## 7. Interior PV

In 3 of the 4 cases considered, the subsurface fields predicted by SQG are qualitatively correct but decay too rapidly with depth. This decay is a direct consequence of assuming the PV is surface-trapped. One can imagine that if the PV extends deeper down, the subsurface flow could be stronger. To examine this, we must consider the particular solution of (4).

Generally, we don't know the subsurface PV; the satellite sees only the surface temperature. However, *if* the subsurface PV could be estimated from the surface density, we could use that PV to derive the particular solution of (4). Lapeyre and Klein (2006) argued that baroclinically unstable flows could produce such a subsurface PV, and proposed a relation between it and the surface density. Then the subsurface fields could again be derived entirely from the surface density.

Hereafter we will use the *in situ* data to seek such a relation empirically. We do this by calculating the subsurface PV in (4) from the *in situ* density, and then calculating a regression, at each depth, between the PV and the surface density,  $\rho_s$ :

$$G(z) \equiv \frac{\iint \rho_s(x, y) Q(x, y, z) dx dy}{\iint \rho_s^2 dx dy}. \quad (9)$$

A similar calculation was made by Lapeyre and Klein (2006). We did this for two of the *in situ* sets and the model data; all three yielded similar results.

Consider the Alboran Sea data first. We will use the shallowest density field from the seaosar data rather than the SST, so that we are only dealing with differences in vertical structure. The regression between the surface density anomaly (the difference from the area-average) and the PV is shown in circles in the left panel of Fig. (17). The regression is positive near the surface, crosses zero at around 80 m and has a minimum at about 160 m. This implies the PV is correlated with the surface density near the surface and anti-correlated deeper down.

One can fit the regression  $G(z)$  satisfactorily using a decaying sinusoidal function:

$$f(z) = a \cos(z/b) e^{z/c}.$$

However, we chose to use an even simpler function, a decaying exponential:

$$f(z) = a e^{z/c}$$

Both functions yield similar corrections to the subsurface density, but we prefer the exponential for its simplicity. Using  $a = 1.7 \times 10^{-4} \text{ m}^3/\text{kg}/\text{sec}$  and  $c = 50 \text{ m}$  yields the solid curve in the left panel of Figure 17. The fit is reasonably good above 100 m, although the minimum at 160 m is missed.

With the regression, we can reconstruct a proxy for the subsurface PV:

$$q_P = f(z) \rho_s.$$

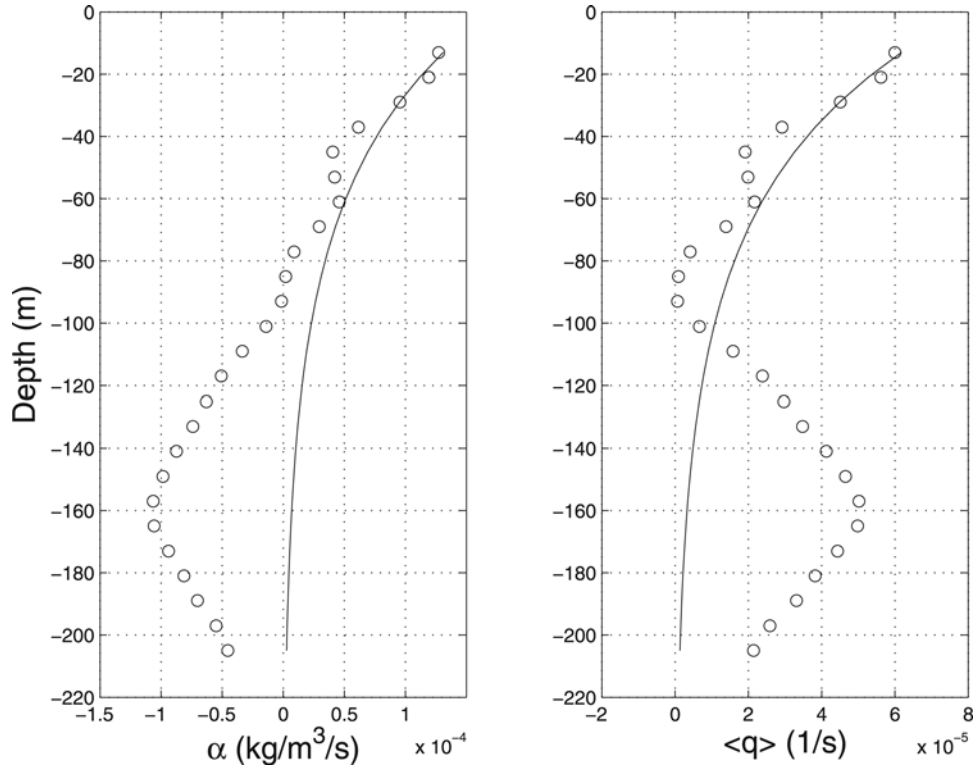


Figure 17. The regression between interior PV and the surface density, averaged over area and plotted against depth (left panel, circles), from the Alboran Sea data. The solid line is an empirical fit, given in the text. The right panel shows the area-average of the absolute value of the PV vs. depth (circles) and the same field using the empirical  $Q - \rho_s$  regression function.

We compare this to the actual PV by averaging the absolute values of both over area, and plotting them against depth (right panel of Fig. 17).<sup>9</sup> Again the agreement is good above 100 m and less good below.

Our primary goal though is the subsurface density field. To obtain this, we incorporate the proxy PV into (4):

$$\frac{1}{\rho_0 f} \left[ \nabla^2 p + \frac{\partial}{\partial z} \left( F(z) \frac{\partial}{\partial z} p \right) \right] = f(z) \rho_s = a e^{z/c} \rho_s \quad (10)$$

and solve for the pressure. As before, we require the solution match the surface density and decay with depth. Again we Fourier transform in the horizontal. The solution, expressed

9. We use the absolute values because the PV derives from the density anomaly. So the area-average of the stretching term is nearly zero.

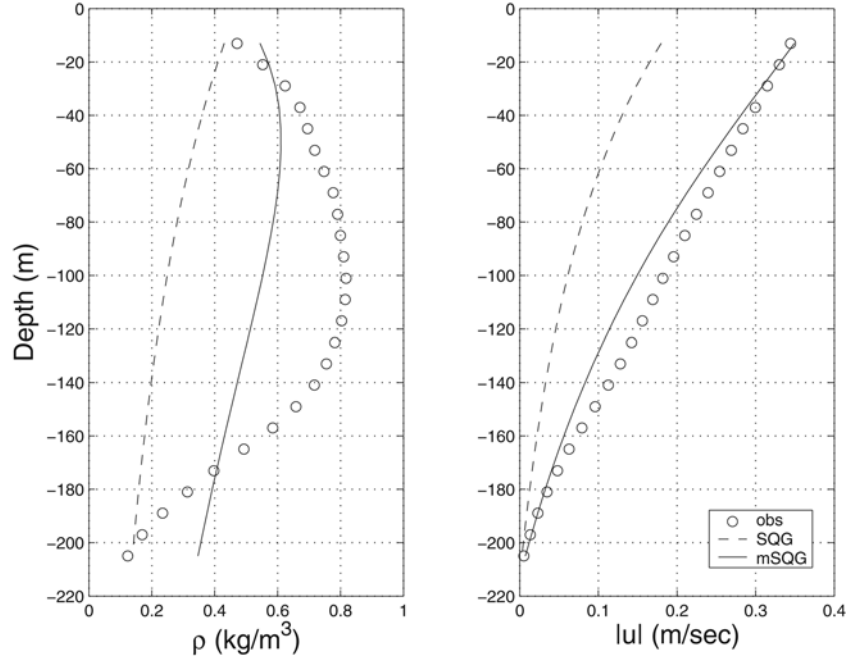


Figure 18. (a) The observed area-averaged, absolute density anomaly vs. depth (circles) from the Alboran Sea data, and that predicted by SQG (dashed line) and by the modified SQG solution (solid line). (b) The corresponding rms velocities.

in terms of the density, is:

$$\rho = \rho_s e^{\kappa z / \sqrt{F}} + \rho_s \frac{\rho_0 a f c}{g(F - \kappa^2 c^2)} (e^{\kappa z / \sqrt{F}} - e^{z/c}). \quad (11)$$

The first term in (11) is just the standard SQG solution. The correction due to the interior PV can either strengthen or weaken the standard solution at a given depth. This depends on the amplitude,  $a$ , but also on the relative sizes of the vertical decay scale of a given Fourier mode and the PV's e-folding scale,  $c$ . Note the second term is infinite if the e-folding scale matches that of one of the Fourier modes, i.e. if:

$$c = \frac{\sqrt{F}}{\kappa}.$$

In that case the singular mode must be treated separately, which is straightforward.

In the left panel of Figure 18, we compare the average density anomaly from observations with those predicted by the standard and modified SQG models. Strikingly, the observations exhibit a mid-depth maximum, at around 100 m; this is why the density anomaly appears to strengthen with depth in Figure 8. The SQG density anomaly (dashed line) instead decays

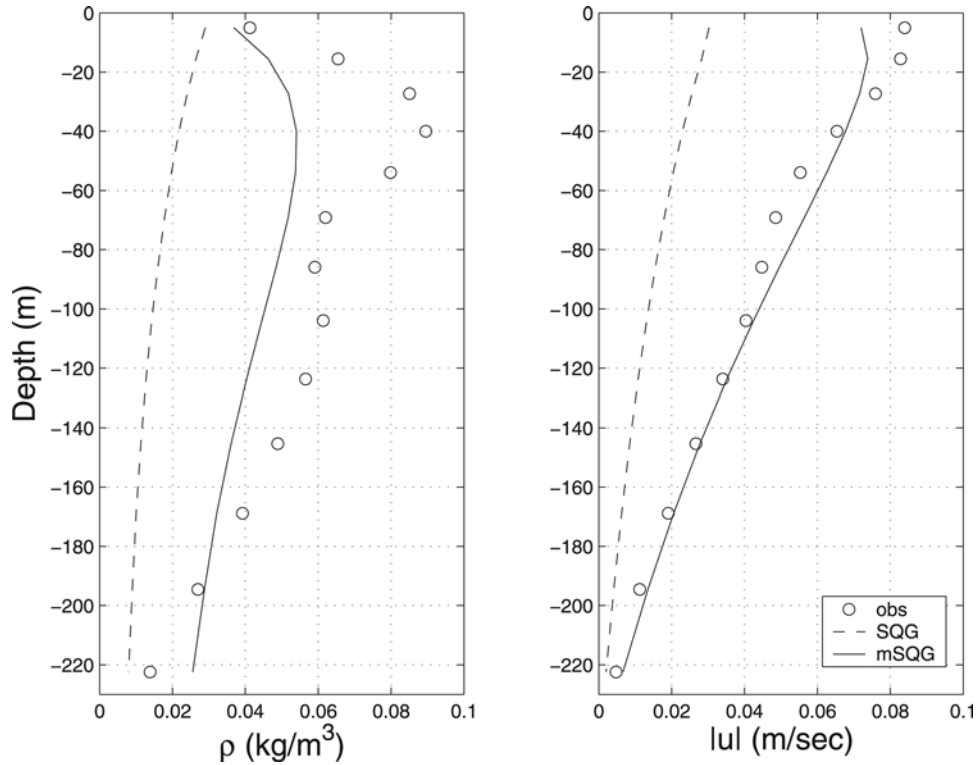


Figure 19. (a) The area-averaged, absolute density anomaly vs. depth (circles) from the model data, and that predicted by SQG (dashed line) and by the modified SQG solution (solid line). (b) The corresponding rms velocities. The data come from the later time in the model simulation, as in Figure 4.

monotonically and is weaker than the observed. In contrast, the density anomaly from the modified SQG model (solid curve) is stronger and also exhibits a mid-depth maximum. However the density anomaly is still somewhat weaker than observed, and the subsurface maximum is somewhat too shallow.

The model is more successful predicting the vertical decay of the horizontal velocities (right panel). The observed velocities decay monotonically with depth, with surface values near 35 cm/sec. The standard SQG velocities have a similar vertical decay but are about half as strong. The modified SQG velocities are much closer to observed. We could of course obtain even better agreement if we tune the function,  $f(z)$ , but this is not the point.

In Figure 19, we compare the density anomaly and the rms horizontal velocities from the model data (Section 3). For this, we used an exponential function  $f(z)$  with an amplitude of  $a = 1.3 \times 10^{-3} \text{ m}^3/\text{kg}/\text{sec}$  and an e-folding scale  $c = 30 \text{ m}$ . Here too the model density anomaly has a subsurface maximum, near 40 m depth (left panel). The density anomaly



from the standard SQG model is again too weak and decays monotonically. The modified SQG solution is nearer the observed curve and also exhibits a middepth maximum, at about the right depth. However, as with the Alboran Sea case, the predicted density anomaly is still somewhat too weak. But the modified SQG velocities on the other hand are fairly close to the observed velocities in strength and vertical decay.

Thus the subsurface density and velocity fields are greatly improved if one includes a proxy for the interior PV. Note that this addition increases the strength of the subsurface flow over that in the standard SQG model, but does not change the subsurface structure. We represented the interior PV as a product of a decaying exponential and the surface density. How one determines the amplitude and e-folding scale of the exponential in application is something that needs to be addressed; we discuss this more below.

## 8. Summary and discussion

We have examined a method for predicting near surface horizontal and vertical velocities from surface temperature data. The method, which derives from the surface quasi-geostrophic (SQG) approximation, requires only SST (assuming that SST reflects the surface density) and a climatological estimate of the background stratification. The standard SQG model assumes that the subsurface PV is uniform (here taken to be zero). We also considered a modified version of the model, in which the subsurface PV is non-uniform and derives from the surface density.

We applied these methods to observations from a three-dimensional model simulation of an unstable front and from three oceanographic surveys of the near-surface density field (off California, in the Alboran Sea and in the Azores Front region). The comparisons suggest the standard SQG model yields qualitatively reasonable velocities in the upper 100–200 m of the water column. However the velocities are consistently too weak. We found that this problem comes from assuming the interior PV is zero. Using the modified SQG model, which includes an interior PV deriving from the surface density, gave more realistic subsurface current speeds.

How reasonable are the various assumptions made with these models? For one, the velocities are assumed to be geostrophic. We could only test this with the ocean circulation model, but geostrophy was very accurate at the scales examined (1–100 km). The assumption that the near-surface flow is dominated by structures visible at the surface was supported in three of the four cases. However in the California Current case, a tongue of cold water below the surface was missed because it had a weak surface signature. Thus the SQG model should be applied in regions where advection dominates temperature changes, for instance near an unstable front. The same applies to the MCC method (Wahl and Simpson, 1990).

The assumption that temperature dominates density was reasonable in the three *in situ* data sets considered here. Of course it will be less reasonable elsewhere, e.g. at high latitudes. However, if sea-surface salinity (SSS) becomes available, the present method could

be used with the resulting surface density. There is the possibility that salinity gradients compensate temperature gradients in the surface mixed layer, yielding near-zero density gradients (Rudnick and Ferrari, 1999). Although density compensation was not seen in the cases considered here, it would seriously affect using temperature to diagnose density. Then one would definitely require surface salinity as well.

As stated, the assumption of a uniform interior PV appears to be inappropriate. Adding an interior PV which derives from the surface density greatly improves the strength of the subsurface response. Doing this does not change the horizontal structure of the subsurface fields, only the amplitude. Even the standard SQG model gave fairly reasonable subsurface structures.

The assumption that the subsurface PV can be derived from the surface density could (and should) be tested by a systematic analysis of climatology and/or reanalysis data. It is entirely possible that this relation varies with region, and that needs to be determined. In their numerical simulation of an unstable jet, Lapeyre and Klein (2006) found that including a proxy for the interior PV caused the subsurface density anomaly to decay *more* rapidly with depth than with the standard SQG model. Their  $Q - \rho_s$  regression exhibited a similar vertical structure to those considered here, but was opposite in sign, so that the shallow PV was anti-correlated with the surface density. If correct, their result could reflect a regional variation, due perhaps to differences in the large scale forcing. One obviously would like to know how common such differences are, since this will affect the application of the modified SQG model.

We represented the  $Q - \rho_s$  regression function,  $f(z)$ , in the simplest way, as a decaying exponential. The actual function in most of our cases was closer to a decaying exponential-sinusoid. Indeed it is not surprising that  $f(z)$ , deriving from the interior PV, should have a more complex shape. Nevertheless, the exponential has only two free parameters, the e-folding scale and the amplitude, which is a decided advantage for the application to real data. In our examples, the e-folding scale could be estimated by examining the background stratification. Choosing the amplitude is more problematic, but in principle this could be done by choosing a value which yields the most reasonable surface velocities. These are admittedly empirical guidelines. Better estimates might come from the proposed study of climatology.

Another improvement on the standard SQG method was proposed by Hakim *et al.* (2002). Their “SQG+1” method retains the first order correction to SQG in Rossby number, with several consequences. The velocities are augmented, and an asymmetry arises in the sign of the vortices. SQG by itself is symmetric in this respect, having equal numbers of cyclones and anticyclones. But SQG+1 produces more cyclones which moreover are more compact and stronger than the anticyclones. A similar asymmetry is observed with vortices on the tropopause, and SQG+1 is a compelling explanation. Interestingly, cyclones are *also* more plentiful in the surface mixed layer (Rudnick, 2001). A potential explanation for this asymmetry is the destabilization of anticyclones by inertial oscillations (Klein *et al.*, 2003). But the asymmetry could also be a signature of SQG+1 dynamics at the ocean surface.

The present model could be useful in two particular applications. For one, it could be used to predict vertical velocities for biology. In all the cases examined,  $w$  was intensified near fronts (see also e.g. Pollard and Regier, 1992; Rudnick, 1996). In many previous physical-biological studies, the focus has been on eddies, which are thought to pump nutrients toward the surface. We have seen the strongest vertical motion occurs rather along the edges of vortices and, moreover, can have both signs (see also Flierl and McGillicuddy, 2002). Due to the marked variations the vertical velocity exhibits in both space *and* time (Section 4), objective methods like the SQG method could be valuable.

Second, we believe the SQG method could be useful for assimilating SST into operational ocean models. Currently SST is projected downward into the interior using empirical relations derived from observed correlations (e.g. Tang *et al.*, 2004). The SQG method instead provides a dynamical basis for this projection, linking the horizontal and vertical scales of motion. Taking it the other way around, assimilating the SQG-derived temperature into an ocean model is likely to provide more realistic fields than with the SQG model alone, because the model can in principle also capture the subsurface fields with little surface signature.

*Acknowledgments.* We are grateful to Kipp Shearman, D.L. Rudnick, P. Velez-Belchi and J. Tintore for graciously sharing their seaosar data, and P. Cornillon and D. Holloway for assisting us with extracting SST data via the Pathfinder program. We thank Guillaume Lapeyre and Patrice Klein for sending us their manuscript prior to publication and Patrice Klein for his detailed reviews. JHL was supported under the Norwegian NOCLIM II project and AM received support from NASA and NOAA.

#### REFERENCES

- Breaker, L. C., D. B. Rao, V. M. Krasnopolsky and X. H. Yan. 1994. The feasibility of estimating ocean surface currents on an operational basis using satellite feature tracking methods. *Bull. Am. Met. Soc.*, 75, 2085–2095.
- Chelton, D. B. and M. G. Schlax. 1996. Global observations of oceanic Rossby waves. *Science*, 272 (5259), 234–238.
- Eady, E. T. 1949. Long waves and cyclone waves. *Tellus*, 1, 33–52.
- Emery, W. J., A. C. Thomas, M. J. Collins, W. R. Crawford and D. L. Mackas. 1986. An objective method for computing advective surface velocities from sequential infrared satellite images. *J. Geophys. Res.*, 91 (C11), 12865–12878.
- Flierl, G. R. 1978. Models of vertical structure and the calibration of two-layer models (for oceans). *Dyn. Atmos. Oceans*, 2, 341–381.
- Flierl, G. R. and D. J. McGillicuddy. 2002. Mesoscale and submesoscale physical-biological interactions, *in* Biological-Physical Interactions in the Sea, *The Sea*, 12, A. R. Robinson, J. J. McCarthy and B. J. Rothschild, eds., John Wiley, NY, 113–185.
- Hakim, G. J., C. Snyder and D. J. Muraki. 2002. A new surface model for cyclone-anticyclone asymmetry. *J. Atmos. Sci.*, 59, 2405–2420.
- Held, I. M., R. T. Pierrehumbert, S. T. Garner and K. L. Swanson. 1995. Surface quasigeostrophic dynamics. *J. Fluid Mech.*, 282, 1–20.
- Holton, J. R. 1992. *An Introduction to Dynamic Meteorology*, Academic Press, 511 pp.
- Hoskins, B. J., I. Draghici and H. C. Davies. 1978. A new look at the omega-equation (for vertical velocity in atmospheric circulation). *Quart. J. Royal Met. Soc.*, 104, 31–38.

- Isachsen, P. E., J. H. LaCasce, C. Mauritzen and S. Hakkinen. 2003. Wind-forced barotropic flow in sub-polar regions. *J. Phys. Oceanogr.*, *33*, 2534–2550.
- Kelly, K. A. and P. T. Strub. 1992. Comparison of velocity estimates from advanced very high resolution radiometer in the coastal transition zone. *J. Geophys. Res.*, *97*, 9653–9668.
- Klein, P., B. L. Hua and X. Carton. 2003. Emergence of cyclonic structures due to the interaction between near-inertial oscillations and mesoscale eddies. *Quart. J. Royal Met. Soc.*, *129*, 2513–2525.
- Kundu, P. K., J. S. Allen and R. L. Smith. 1975. Modal Decomposition of the velocity field near the Oregon coast. *J. Phys. Oceanogr.*, *5*, 683–704.
- Lapeyre, G. and P. Klein. 2006. Dynamics of the upper oceanic layers in terms of surface quasi-geostrophy theory. *J. Phys. Oceanogr.*, *36*, 165–176.
- Mahadevan, A., J. Oliger and R. L. Street. 1996. A non-hydrostatic mesoscale ocean model, Part 1: Well-posedness and scaling. *J. Phys. Oceanogr.*, *26*, 1168–1880.
- McPhaden, M. J. 1993. TOGA-TAO and the 1991–93 El Niño-Southern Oscillation event. *Oceanography*, *6*, 36–44.
- Pauley, P. M. and S. J. Nieman. 1992. A comparison of quasigeostrophic and nonquasigeostrophic vertical motions for a model-simulated rapidly intensifying marine extratropical cyclone. *Mon. Weather Rev.*, *120*, 1108–1134.
- Pedlosky, J. 1987. *Geophysical Fluid Dynamics*, Springer, 728 pp.
- Pollard, R. T. and L. A. Regier. 1992. Vorticity and vertical circulation at an ocean front. *J. Phys. Oceanogr.*, *22*, 609–625.
- Rudnick, D. L. 1996. Intensive surveys of the Azores front 2: Inferring the geostrophic and vertical velocity fields. *J. Geophys. Res.*, *101*, 16,291–16,303.
- . 2001. On the skewness of vorticity in the upper ocean. *Geophys. Res. Lett.*, *28*, 2045–2048.
- Rudnick, D. L. and R. Ferrari. 1999. Compensation of horizontal temperature and salinity gradients in the ocean mixed layer. *Science*, *283*, 526–529.
- Rudnick, D. L. and J. R. Luyten. 1996. Intensive surveys of the Azores front 1: Tracers and dynamics. *J. Geophys. Res.*, *101*, 923–940.
- Shearman, R. K., J. A. Barth and M. P. Kosro. 1999. Diagnosis of the three-dimensional circulation associated with mesoscale motion in the California Current. *J. Phys. Oceanogr.*, *29*, 651–670.
- Stammer, D. 1997. Global characteristics of ocean variability estimated from regional TOPEX/POSEIDON altimeter measurements. *J. Phys. Oceanogr.*, *27*, 1743–1769.
- Tang, Y., R. Kleeman and A. M. Moore. 2004. SST Assimilation experiments in a tropical Pacific Ocean model. *J. Phys. Oceanogr.*, *34*, 623–642.
- Tintoré, J., D. Gomis, S. Alonso and G. Parrilla. 1991. Mesoscale dynamics of vertical motion in the Alborán Sea. *J. Phys. Oceanogr.*, *21*, 811–823.
- Vélez-Belchí, P., M. Vargas-Yáñez and J. Tintoré. 2005. Observation of a western Alborán gyre migration event. *Prog. Oceanogr.*, *66*, 190–210.
- Viudez, A., R. L. Haney and J. Tintore. 1996. Circulation in the Alboran Sea as determined by quasi-synoptic hydrographic observations. Part I: Three-dimensional structure of the two anticyclonic gyres. *J. Phys. Oceanogr.*, *26*, 684–705.
- Wahl, D. D. and J. J. Simpson. 1990. Physical processes affecting the objective determination of near-surface velocity from satellite data. *J. Geophys. Res.*, *95*, 13,511–13,528.
- Zavialov, P. O., J. V. Grigorieva, O. O. Moller, A. G. Kostianoy and M. Gregoire. 2002. Continuity preserving modified maximum cross-correlation technique. *J. Geophys. Res.*, *107* (C10), 10.1029/2001JC001116.

Received: 17 August, 2005; revised: 19 June, 2006.

